# Optical Characterisation of small surface targets

Piet B.W. Schwering[1], Dirk F. Bezuidenhout[2], Willem H. Gunter[3], Arie N. de Jong[1], Peter J. Fritz[1], Francois P.J. le Roux[2], Rheinhardt H. Sieberhagen[2], Mark Holloway[2], George Vrahimis[3], Faith J. October[3], Rob A.W. Kemp[1]

[1]TNO Defence, Security and Safety, P.O. Box 96864, NL-2509 JG The Hague, Netherlands, piet.schwering@tno.nl
[2]CSIR DPSS, P.O. Box 395, Pretoria, 0001, South Africa, dbezuide@csir.co.za
[3]Institute for Maritime Technology (IMT), Martello Road, Simon's Town 7995, South Africa, whg@imt.co.za

## ABSTRACT

Present-day naval operations take place in coastal environments as well as narrow straits all over the world. Coastal environments around the world are exhibiting a number of threats to naval forces. In particular a large number of asymmetric threats can be present in environments with cluttered backgrounds as well as rapidly varying atmospheric conditions. In these conditions the threat contrast may be low and varying, and the amount of background clutter can be severe. These conditions require the electro-optical means of detection and classification to be optimized in order to have more time to act against threats. In particular the assessment of classification means is an important issue. Beside short-range coastal paths, long-range horizontal paths with variable atmospheric conditions are of interest. The small differences between types of vessel can help us determine the classification of the vessel type. Different payloads and people on-board can be clues to the classification of the vessel. Operations in warmer environments, limiting the atmospheric transmission due to water vapour absorption, are challenging. Understanding of the impact of the different environments on the optical characteristics of threats is of great importance. For this purpose a trial was planned to assess the optical characteristics of different types of small surface vessels in a coastal environment. During this trial a number of small targets were used during different parts of the day and night. Furthermore positional as well as atmospheric characterisation was performed as ground truth information. From this data a first analysis was performed showing strong intensity fluctuation in target as well as background signal levels. At longer ranges and in coastal environments these target signals may well be hidden within the background clutter. This data is essential to feed models for the assessment of sensor performance in coastal environment.

**Keywords:** Electro-optical systems, system concepts, target contrast, signatures, detection and classification.

## 1. INTRODUCTION

Present-day naval operations take place in coastal environments, wide bays as well as narrow straits all over the world. These environments exhibit a number of threats to naval forces (threats such as divers, surface and underwater objects, missiles and lasers). In particular, a large number of asymmetric threats may be present in environments with highly cluttered coastal backgrounds as well as rapidly varying atmospheric conditions. In these conditions the threat's contrast may be low and varying, and the amount of background clutter can be severe. In coastal environments electro-optical means of detection and classification should be optimized in order to have more time to act against threats.

Electro-optical sensor suites on-board of naval vessels are used for different tasks as detection, classification and identification (Schwering *et al.*[1]). Improved situational awareness can be achieved by means of passive electro-optical systems, such as infrared and visible light sensors. For long-range detection capability, elevated sensor masts and flying platforms are ideally suited for the surveillance task and improve the operational picture. A primary issue is the incorporation of new electro-optical technology and signal processing into the new system concepts. The derivation of information from the high spatial resolution imagery created by the sensors is of great importance. As electro-optical sensors do not have all-weather capability, the performance degradation in adverse scenarios should be understood, to support the operational use of adaptive sensor management techniques.

Apart from the naval scenario, algorithms have been developed for detection of threats in land scenarios. For detection the algorithms make use of different kinds of target features, such as hot spots, motion, and structure. Algorithms for adaptive sensor management are being tested using live recordings from naval operations. Incorporating these algorithms into new types of Electro-optical (EO) system concepts, based on infrared and visible light systems as well as integrated systems, is foreseen.

Electro-Optical Remote Sensing, Detection, and Photonic Technologies and their Applications
edited by G. W. Kamerman, O. K. Steinvall, K. L. Lewis, K. A. Krapels, J. C. Carrano, A. Zukauskas
Proc. of SPIE Vol. 6739, 67390H, (2007) · 0277-786X/07/$18 · doi: 10.1117/12.738507

In this paper we present first results from trials and analysis of accurate target signature contrasts of different vessels under different atmospheric conditions. The atmospheric and background influence are discussed.

## 2. TRIAL OVERVIEW

The objective of our research is to determine contrast and contrast variability of different small vessels in electro-optical wavebands and determine optimum sensor concepts for applicability against the small target threats (Schwering[2]). These contrasts should lead to information of the optical characteristics of the vessels. For this purpose we performed a trial from 4-15 June 2007 in Simon's Town, False Bay, South Africa.
For analysis a number of targets was used, namely a small scientific work boat, a small harbour patrol boat, a jetski, a rigid hull inflatable boat, a wooden whaler and swimmers. Images of the small scientific work boat, the small harbour patrol boat and the jetski are shown in Figure 1. With these vessels patterns were sailed inbound and outbound, with vessels circling at a fixed number of defined positions. These circles are ideal to investigate the aspect angle variation, while the inbound runs can be used for assessment of the range dependence of the threat contrast.

*Figure 1: Visual imagery of some of the target vessels: small scientific work boat, small harbour patrol boat and jetski.*

Day and night recordings were planned to obtain a large variety of target contrasts. A number of different vessels were planned during the trial to assess the variability of the targets and target features as well as the detectability differences for different types of targets. Target reconnaissance depends on the spatial resolution of imaging sensors. A number of different sensors were therefore used. These sensors were selected to support analysis of the data in the field of Infrared Search and Track (IRST) detection systems, electro-optical tracking by infrared and visual cameras, as well as to support sensor fusion studies. A list of imaging sensors used for target and background characterisation in the trial is presented in Table 1.

*Table 1: Imaging sensors used during the trial for recording target optical characteristics.*

| ***Sensor*** | ***Wavelength*** | ***FOV (°)*** | ***IFOV (mrad)*** | ***NETD*** | ***Comment*** |
|---|---|---|---|---|---|
| | | | | | |
| Marlin AVT F-033B | 0.4-0.7 µm | 0.92x0.67 | 0.025 | - | Progressive Scan camera |
| SU-1.7 | 1.0-1.7 µm | 3x4 | 0.22 | - | InGaAs detector, 320x240 |
| Imspector | 0.4-0.9 µm (90 bands) | 2.4 – 24 | 0.07 – 0.7 | - | Hyperspectral imager. Resolution approx. 10 nm |
| Polarisation camera | 0.4-0.7 µm | | | - | RGB colour, rotating polariser (period 7 sec). |
| | | | | | |
| Cedip Jade SWIR | 1.0-2.5 µm | 5.5x4.1 | 0.25 | - | 320x256 CMT detector |
| Cedip Jade MWIR | 3.5-5.1 µm | 5.5x4.1 | 0.25 | 20 mK | 320x240 CMT detector |
| Cedip Jade VLWIR | 7.8-12.0 µm | 5.5x4.1 | 0.25 | 25 mK | 320x240 CMT detector |
| Prosilica | 612-652 nm | 10.8x5.4 | 0.184 | - | Visual band imager |
| | | | | | |
| CEDIP JADE MWIR | 3.6-5.0 µm | 2.75x2.06 | 0.15 | 25 mK | 320x240 InSb FPA |
| Agema THV1000 CLR | 7.2-12.6 µm | 3.1x2.4 | 0.09 | 100 mK | 6 element SPRITE–scanning system. |
| OPTOCON LWIR Uncooled | 8-14 µm | 5.6x4.2 | 0.3 | 150 mK | 320x240 Amorphous Si FPA |
| Arecont AV5100M CCD | 0.4-0.8 µm | 4.4x3.3 – 1.1x0.82 | 0.03 – 0.007 | - | High resolution, 5Mpixel CCD. Used focal length 75, 100, 200, 300 mm |

The image data that has been recorded will be used to improve and test image conditioning algorithms (Schutte *et al.*[3]) as well as detection and classification algorithms (van den Broek *et al.*[4]). Application of these techniques could be implemented in sensor fusion systems (such as described in Theil *et al.*[5]).
In Figure 2 we present the location of the trials in False Bay (South Africa). The standard test runs were defined as small circles at 1, 2, 3, 5 km distance from IMT (Institute for Maritime Technology) in Simon' Town, in-bound head-on runs, as well as in-bound and out-bound weaving zig-zag runs. Target positions were accurately measured with a Differential GPS (DGPS) system. In some cases adaptations and extensions of these runs were performed.

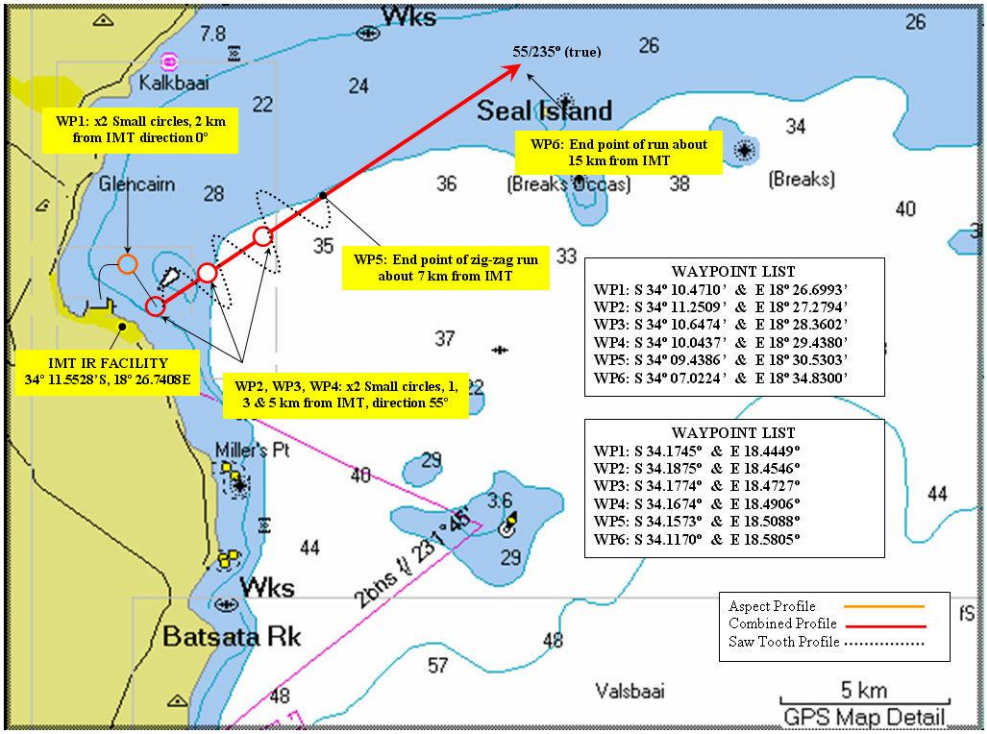


*Figure 2: Overview of the basic tracks and way points (WP) sailed for each of the vessels (map produced with Garmin MapSource).*

Besides imaging sensors, additional equipment was used for characterisation of the environment. These consisted of three meteorological stations, a visibility sensor, two sea water temperature sensors, a turbulence measurement camera (1250 mm Celestron, equipped with a CCD), transmission and scintillation equipment (TNO MSRT at 0.6, 0.9, 1.5 µm) both over 9.7 km, and a Theodolite refraction sensor (Topcon AT-G2 plus CCD) over 15.7 km were used. Scintillation measurements were also done between the IMT Building and the Roman Rock Light House, a distance of 1830 m, using a source containing light emitting diodes centred at 630 nm.
As the data analysis has just started, we present in the following sections the results from the preliminary data analysis.

## 3. TARGET CONTRAST

The EO-system should be designed with the objective that it should be able to detect and classify small surface targets. These processes are very dependent on contrast of the target with respect to the background. For this purpose a description of target features is of extreme importance. Therefore the first stage of our investigation is related to target signatures and the derivation of optical characteristics.
Figure 3 shows some data of one of the targets, the small scientific work boat, recorded during the trials at infrared wavebands. In the figure the bow, stern, port and starboard sides are visible respectively in the 3-5 µm band at a distance of 1 km. In the images lighter grey scales indicate higher temperatures. We observe hot spots due to high temperatures and also due to solar reflection. Additionally cold sky reflection can be seen in the front view in particular. Several parts of the structure of the vessel are clearly visible as well as wake-like features on the sea surface. On the wake additional solar reflections are observed.

*Figure 3: The small scientific work boat recorded in the 3-5 μm band at a distance of 1km (bow-upper left, stern-upper right, port-lower left, and starboard-lower right).*

Intensity polar diagrams of the small harbour patrol boat are presented in Figure 4. Spikes in the contrast intensity polar plots were mainly caused by variation in the target area due to sea spray (boat's pitching action) and wake size. The thermal contrast is higher in the LWIR, with similar signal-to-noise ratios (defined as the difference between the target and background radiance divided by the standard deviation of the background radiance). Sun glint was not a problem in this run.

These results clearly show the strong dependence of the target contrast with various parameters. For small surface vessels the wake can be a dominant feature for detection. The wake length is very dependent on vessel speed and sea state. The wake intensity depends on the difference between the true sea temperature and the apparent sea temperature, with hot spots occurring due to solar reflection. The presence of a wake in image areas close to the target used as the background by detection filters could make the vessel less detectable. Therefore this should be avoided. All reflection features depend on the observed target-sun reflection geometry and on cloud coverage. Furthermore these factors also influence the hot spots generated by sun heating. Clearly a high variability of the target contrasts may be expected.

Figure 5 shows a comparison of target contrast in four different spectral bands under two different environmental conditions. The data on the left was captured on an overcast day, the middle data on a sunny day, while the data on the right was captured under partially sunny conditions. The data was captured at approximately the same time of day. The target was a small scientific work boat making a circle run at a distance to the sensor of approximately 1 km. This boat is characterized by flat, white, specular surfaces and windows. The large contrast variations in the visual and short-wave infrared bands are due to the amount of reflected light changing with aspect angle. The Contrast ratio was calculated as *(Average Target Intensity - Average Background Intensity)/(Average Target Intensity + Average Background Intensity)*. This gives us positive and negative contrasts. Note the spectral differences as well as the difference in overcast and sunlit situations. Infrared contrasts are near zero due to the high background levels. In the figure the following aspect angle axis if used: bow at 0º, starboard at 90º, stern at 180º and port at 270º.

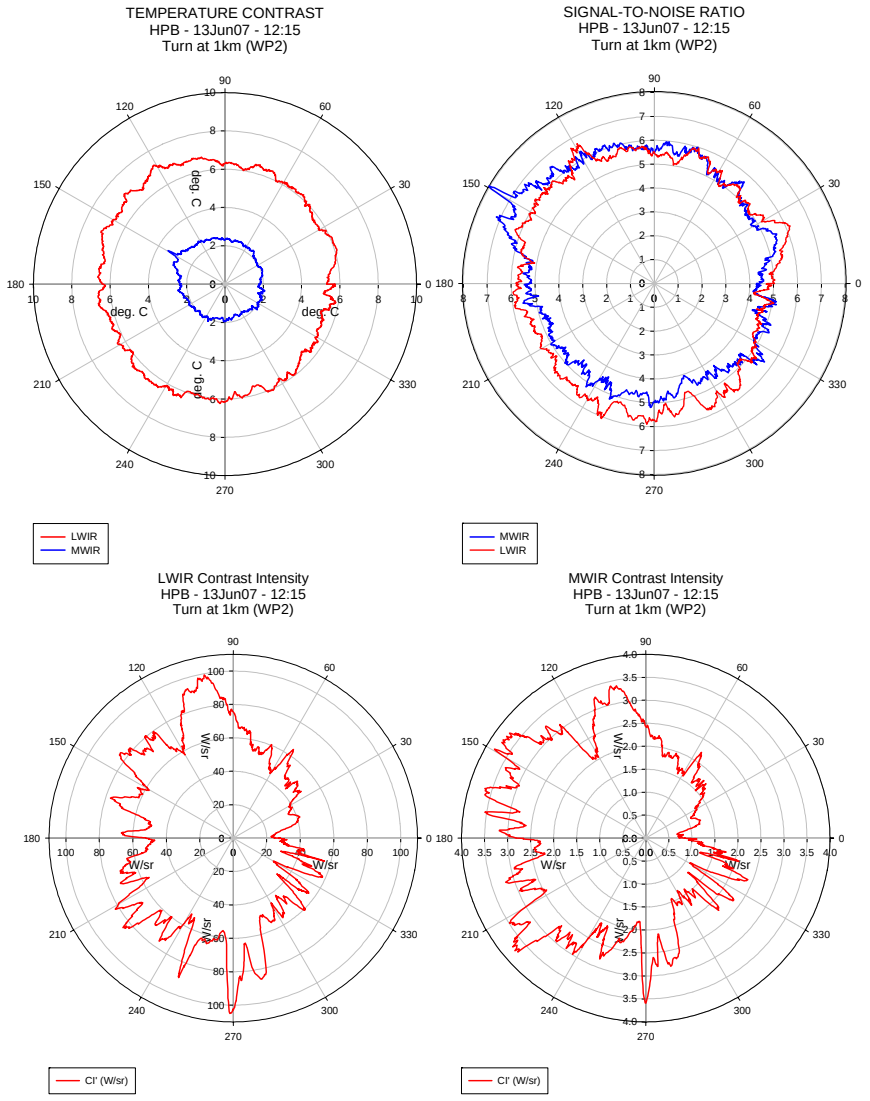


*Figure 4: MWIR & LWIR infrared signature polar plots of small harbour patrol boat (HPB) at 1 km (day time). Apparent temperature contrast (top left), SNR (top right), LWIR contrast intensity (bottom left) and MWIR contrast intensity (bottom right). Boat bow is at 0º and port side is at 90º.*

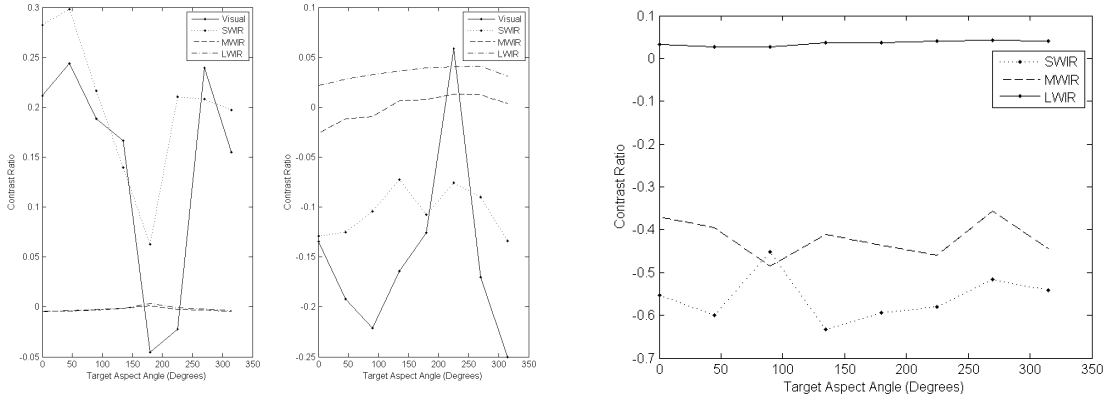


*Figure 5: Target contrast in different spectral bands, with overcast (left), sunlit (middle), partial sun light (right).*

During an inbound run of the small harbour patrol boat a higher thermal contrast, SNR and contrast intensity was obtained in the LWIR compared to the MWIR. This is presented in Figure 6. The fluctuations in the signature were mainly caused by varying amounts of sea spray due the small surface vessel's pitching action. This is also the main contribution to the IR signature at long range and is quite characteristic of a closing small surface target. Sun glint was not a problem in the MWIR in this case (relative sun azimuth angle of about 50º).

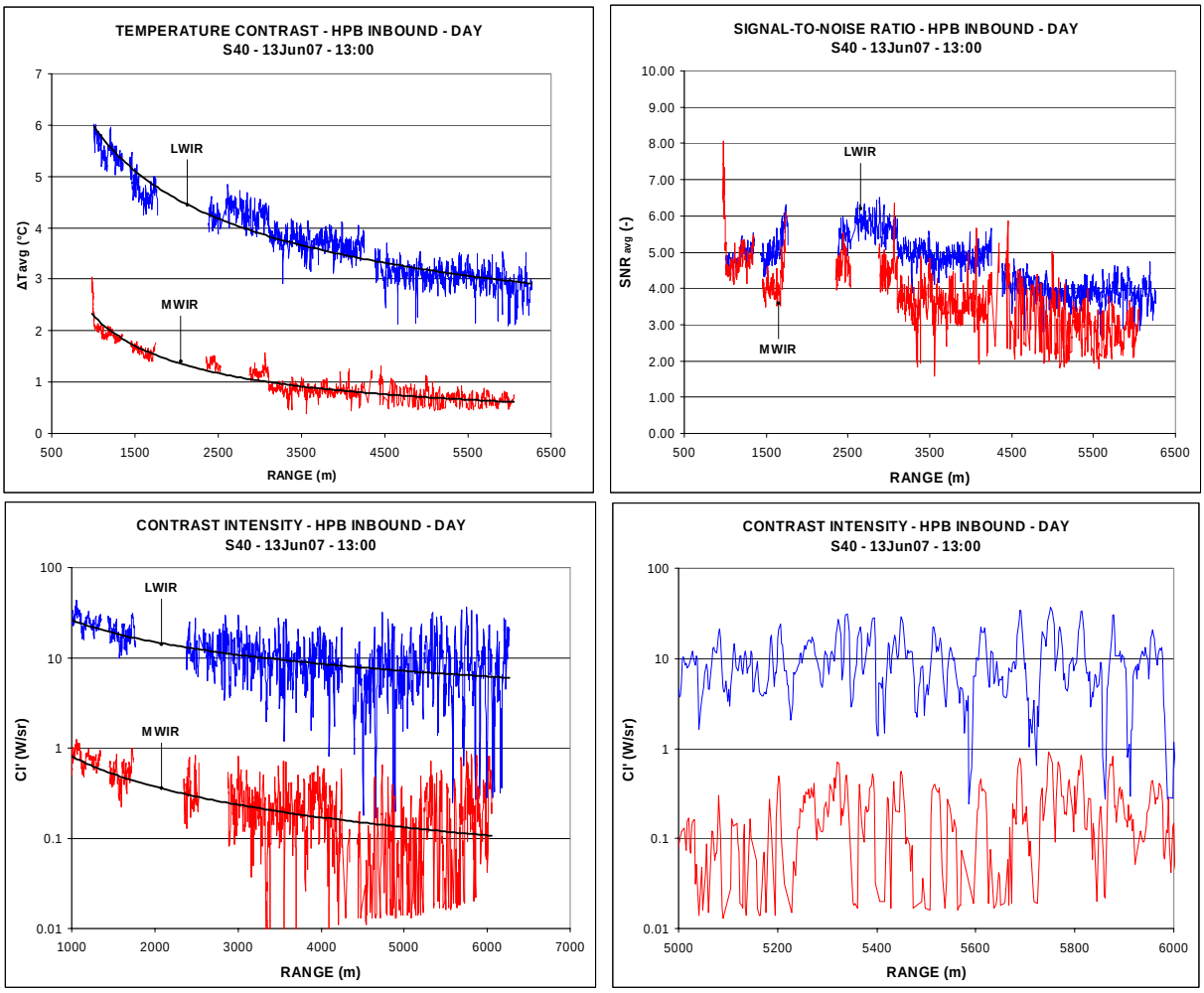


*Figure 6: Measured infrared signature plots of a small harbour patrol boat (HPB) during an inbound run in the MWIR and LWIR (as function of range, during day time). Apparent thermal contrast (top left), SNR (top right) and contrast intensity (bottom left and right) is shown. The bottom right contrast intensity plot's range scale is stretched to show the intensity fluctuations more clearly.*

In Figure 7 we show the measured signature plots for an inbound zig-zag run of the small harbour patrol boat. The change in direction of this boat during a zig-zag inbound run is clearly visible in the MWIR and LWIR measured signature plots due to a higher IR signature on starboard side (negative aspect angles). A better thermal contrast was obtained in the LWIR, but with a decreasing difference as function of increasing range compared to the MWIR. Smaller differences were observed in the SNR. Fluctuations in the contrast intensity plot were mainly caused by variations in the target area due to sea spray generated by the boat's pitching action going through the sea swells (more pronounced at longer ranger).

## 4. BACKGROUND CLUTTER

Of major interest in development of automatic detection and classification systems is the signal processing and how this handles the background. The background has a large influence on the contrast and structure information is normally

better visible in the processed imagery, due to the application of matched filters, hence improving operator aided classification and classification ranges. Background features could then hamper detection.

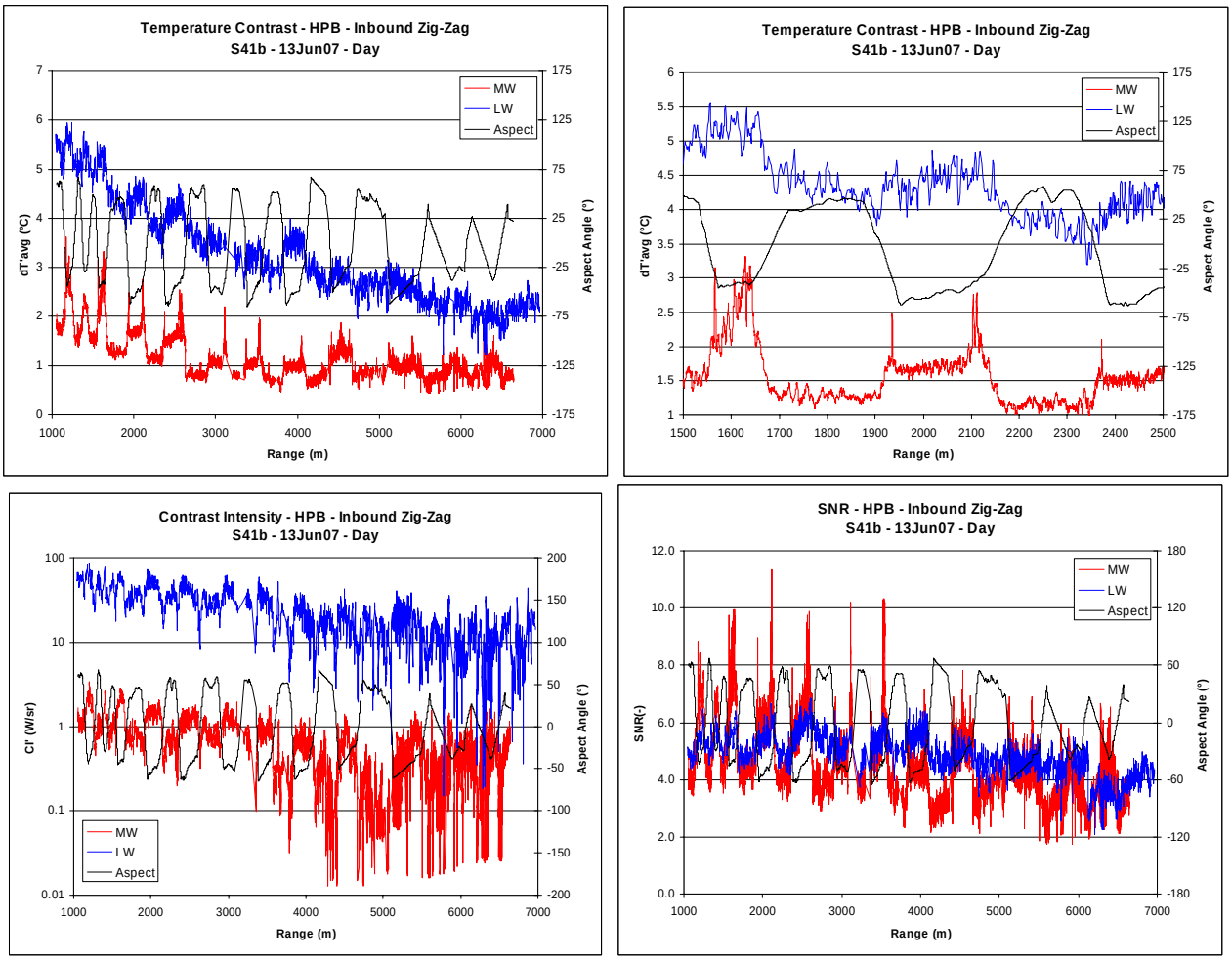


*Figure 7: Measured infrared signature plots of a small harbour patrol boat (HPB) during an inbound "zig-zag" run in the MWIR and LWIR (as function of range, during day time). Apparent thermal contrast (top left and right), contrast intensity (bottom left) and SNR (bottom right) is shown. The range scale in the top right-hand plot is stretched to show the difference between the port and starboard contrast more clearly. Aspect angle is also shown (positive aspect angles for port side).*

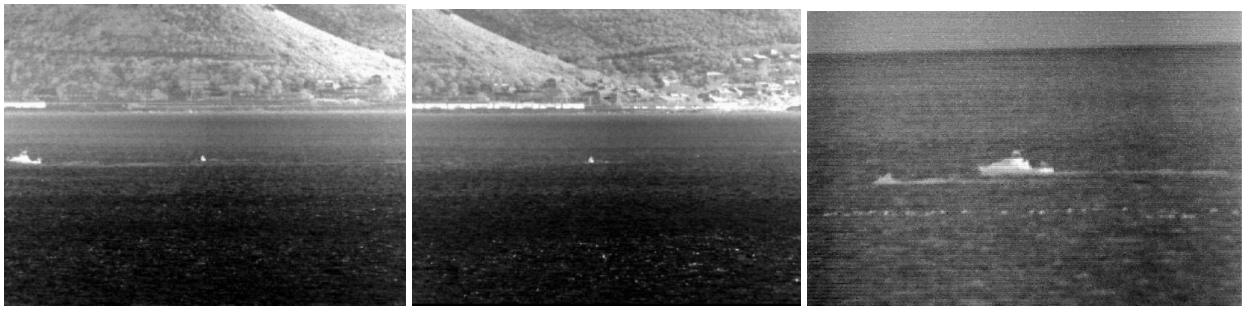

*Figure 8: Small harbour patrol boat and jetski (left), Jetski (middle) both at 2 km, 3-5 μm in a highly cluttered coastal background; Jetski and small harbour patrol boat with wakes and birds in a sea background 8-12 μm.*

In the background a number of different features could influence detection. The processing should look into discrimination between target and background of intensity differences at the spatial, temporal and spectral levels of the data. Detection based on these differences is hampered by the presence of sea structures, ship's wakes, sky and cloudy backgrounds, coastal backgrounds (urban and rural), rocks and light houses, ships and sun glint. In this section we proceed with the analysis of these features.
In Figure 8 we present two images of a jetski against a coastal background. The jetski is clearly visible in the sea, but the high intensity of the coastal area would make the contrast small against the coastal background. The background shows rural and urban areas against a hill, with motorized transport activities present near the coast line. In the left image the small harbour patrol boat is present. The images also show clear wake patterns from the vessels. These patterns are influenced by target speed, sea state and observer position. The intensity and size off these wake patterns can be such that detection can be dominated by it in a positive sense, but also in a negative sense when the wake enters the background window of automatic detection algorithms. The images illustrate the strong dependence of the target contrast on the background. The presence of birds could lead to false alarms in the automatic detection processes.

*Figure 9: Visible light polarisation imagery of the small scientific work boat. Left horizontal, right vertical polarisation.*

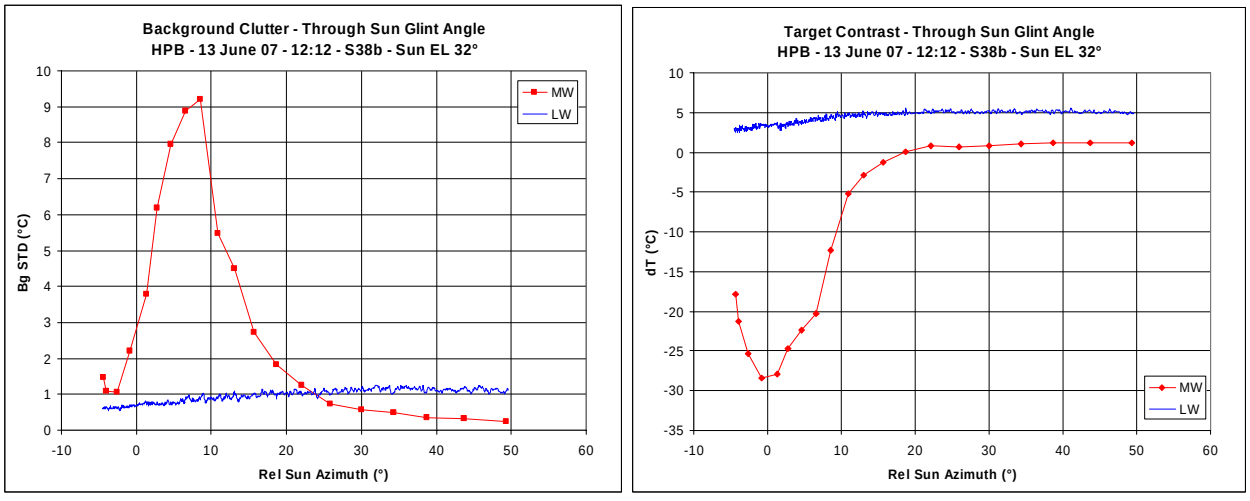


*Figure 10: Measured MWIR and LWIR thermal contrast of a small harbour patrol boat(HPB) and standard deviation in the sea background as function of relative sun azimuth angle (going through the sun glint angle).*

In Figure 9 we present first results from the polarisation camera. This camera can be used to differentiate between reflection on targets and on sea backgrounds. Therefore it is expected that these polarization images can reduce clutter

that is induced by sky and in particular sun glint. We have made use of a rotating polarisation filter, with a period $(max_h\text{-}max_h)$ of approximately 4 s. In Figure 9 we present the minimum intensity and the subsequent maximum intensity. In the image on the left we observe the vessel, strong white caps and spots of sun glint that may hamper detection and certainly could result in false alarms. Some spatial blur is present in the maximum image due to slight positioning errors of the filter). In the image on the right all sun glint spots have been removed, resulting in an image of the vessel with only a few white caps present. It is clear that a large amount of sun glint clutter has been removed, showing the effectiveness of the polarisation approach for clutter rejection in this case.

The strong effect of sun glint on MWIR sensors is clearly demonstrated by Figure 10. The target's MWIR thermal contrast changed from a big negative value (< -28ºC, sensor did saturate) at zero degree relative sun azimuth angle (looking into the sun), to a zero contrast at about 19º and to a positive contrast of 1.2 ºC at a 50º relative sun azimuth angle. In contrast to this the LWIR thermal contrast only changed by 2ºC (from +3 to +5 ºC) going through the sun glint angle. Looking at the standard deviation in the MWIR sea background (measure of the amount of background clutter) the clutter peak was reached at a relative sun azimuth angle of about 8.5º, while the sea background clutter in the LWIR remained fairly insensitive to the relative sun azimuth angle. The range and aspect angle of the target varied between 2.2 to 1.05 km and -28 to -83º (starboard side) from start to the end of this run.

## 5. ATMOSPHERIC CONDITIONS

During the trials meteorological data was recorded at three locations: at the IMT building on the ground floor and on the roof, and at the Roman Rock lighthouse at 1.8 km distance in the bay. Visibility was recorded on the IMT roof, and sea water temperatures were recorded at two buoy locations at 0.5 and 1.9 km from IMT. For measuring the atmospheric effects transmission measurements and scintillation measurement were performed with the MSRT transmissometer over a 9.7 km path from IMT to Muizenberg. Scintillation and beam wander data was recorded over the same path (but the other way around) to the IMT ground floor and roof. Additional scintillation measurements were taken over a path of 1.8 km from Roman Rock to IMT. Refraction images were recorded in the path from the National Sea Rescue Institute (NSRI) to IMT's ground floor, as well as from Muizenberg to IMT. First results from the experiments are given in the sections below.

Results on previous studies in the field of transmission and refraction measurements over different bays can be found in de Jong *et al.*[6,7]. Beside the atmospheric effect the scintillation data on point sources also give valuable information on the effects on small point sources at long range (such as missiles).

In Figure 11 we present an overview of the global meteorological conditions during the trials. Sunny periods were in the weekend of 3 June and on 12-13 June. In between sunshine, cloudy and rainy conditions were intermittent. This resulted in general in a wide variety of conditions, both for atmospheric transmission and turbulence, as well as for infrared background clutter.

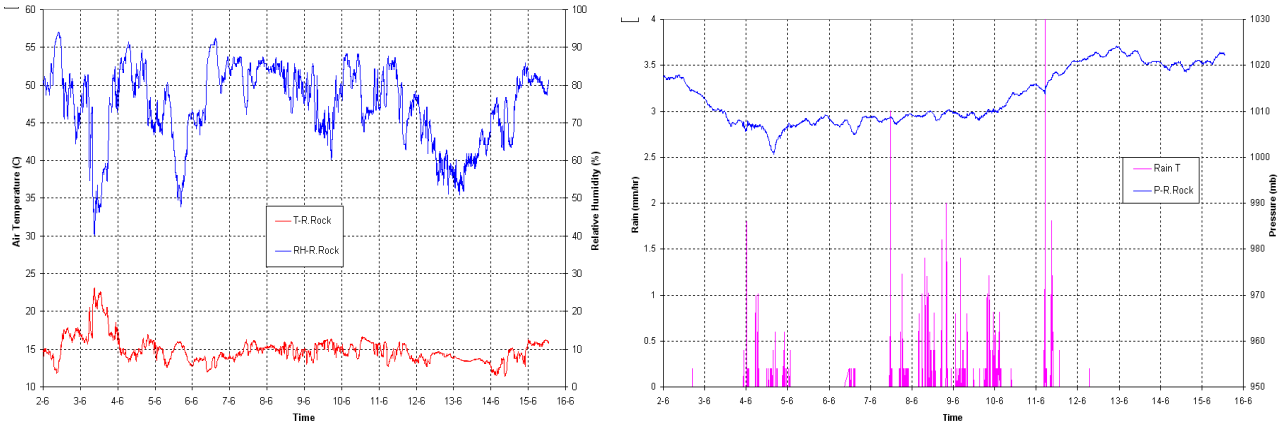


*Figure 11: Meteo recordings from Roman Rock at 1.8 km from IMT for the entire trial period (left air temperature and relative humidity; right pressure and rain rate).*

## 5.1. RESULTS FROM MSRT TRANSMISSOMETER

The Multi-Spectral Radiometer Transmissometer (MSRT) has recently been used for characterization of aerosols in areas along the US West-Coast. During these campaigns, the integration time, used in each of the spectral bands was about 1 second. In the case of the False Bay we wanted to collect data on the aerosol characteristics as well as on scintillation. For this reason we used the channels with the best signal-to-noise ratio: 0.57-0.65 µm, 0.78-1.04 µm and 1.39-1.67 µm. The predicted signal-to-noise ratios in these bands for a range of 9.7 km, an integration time of 10 ms, an atmospheric transmission of 1 and a 100 Watt lamp are respectively 227, 1239 and 947. The chopper frequency was set to 1000 Hz, simultaneously transmitted by a radio link from the IMT building to the receiver station in room E113 in the Empire apartment building in Muizenberg. The heights of the transmitter and receiver above the water level were about 8.1 and 8.0 m. The maximum sampling speed of our data logger was limited to 30 Hz; nevertheless this speed resulted in a data set of 7.8 MB per day. The transmission data were calibrated by using the signal levels during a period of very good visibility (5 June 17.00), while running Modtran for the weather conditions at this time.

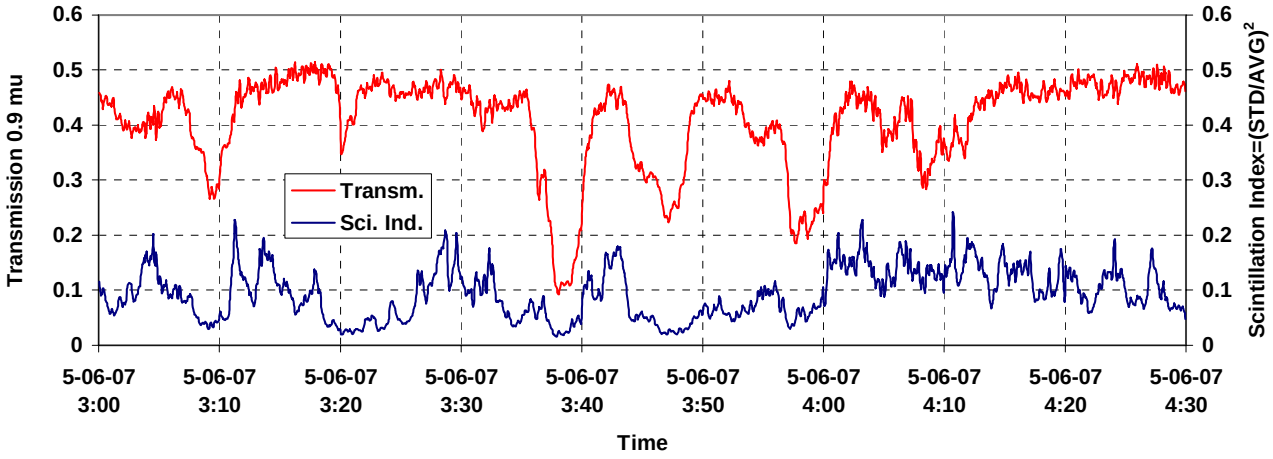


*Figure 12: Example of MSRT data on transmission and scintillation index during the night of 5 June with rain showers.*

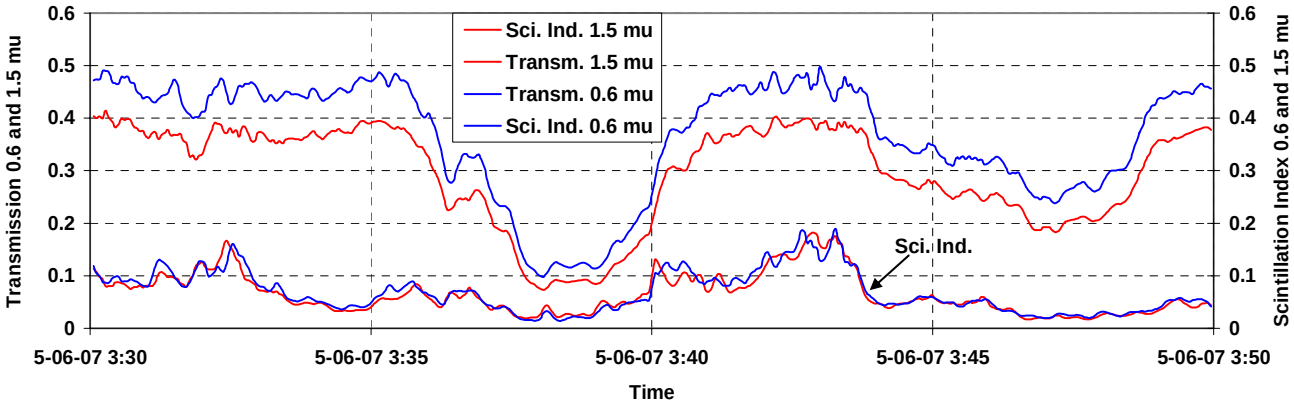


*Figure 13: Close up of τ and SI data for two wavelength bands, showing strong correlations between the bands.*

A sample of the transmission data is shown in Figure 12, taken during a night with rain showers (5 June). For the transmission plot the raw data were averaged over a period of 10 seconds and sampled every 3.3 seconds. The standard deviation of the transmission data was taken for 300 samples of the raw data, subsequently averaged over a 10 second period and sampled every 3.3 seconds. The plots show the tendency that during showers the scintillation index (*SI*) decreases simultaneously with the transmission ($\tau$). Figure 13 shows for part of the period presented in Figure 12 a very strong correlation between $\tau$/*SI* plots in different spectral bands. The value of *SI* is nearly the same in different bands, while the $\tau$ level in the 1.5 µm band is lower than in the 0.6 µm band due to stronger molecular extinction. The level of *SI* stays below 0.3, indicating that the scintillation was not saturated.

The transmission data collected in the period, shown in Figure 13, are plotted against each other in Figure 14 (left). The data follow straight lines with regression coefficients of 0.98 for the plot of 0.9 versus 0.6 µm and 0.86 for the plot of 1.5 versus 0.6 µm. If we remove the effect of molecular extinction and extinction by residual aerosols, both regression coefficients are approaching the value of 1, indicating that the rapid extinctions for several minutes are due to rain somewhere in the measurement path. We have to remember, that the extinction coefficient by rain droplets is nearly independent of wavelength due to the large size of the water droplets compared to the wavelength. Also the correlation of transmission data for a shorter period of 10 seconds during the 20 minutes period of Figure 13 has been carried out. The result for the bands 1.5 and 0.6 µm is shown in Figure 14 (right), together with the transmission plot of $\tau$=0.9 µm. It is found that, even for the short correlation time, the transmission data correlate quite well during rain, even though the spatial separation of the pupils is 11.5 cm. This indicates that the coherence length $r_0$ of the intervening turbulence during rain exceeds this separation distance. The correlation behaviour of the other spectral band combinations is very similar.

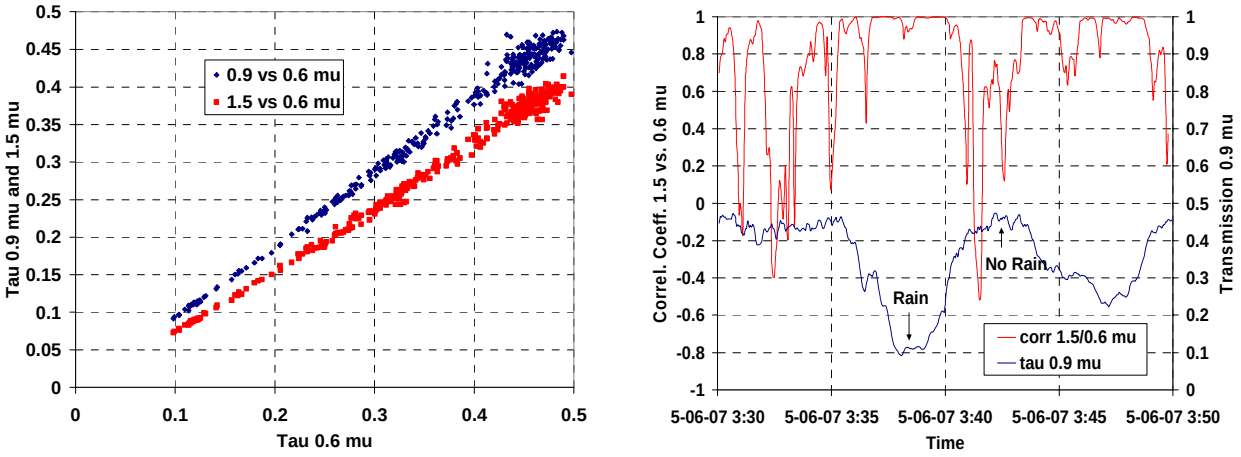


*Figure 14: Correlation of τ data for the period of Figure 13 (20 minutes, left) and for data periods of 10 seconds (right).*

In a further elaboration on the difference in transmission behaviour in rain and without rain conditions, we show the histograms of the samples of the 0.9 µm band, taken in periods of about one minute, in Figure 15 (left). Not only the width of the histograms in both cases, compared to the mean values (equivalent to the root of the scintillation index), is quite different, but also the ratio of the maximum and minimum sample values. For no-rain conditions we find more than a factor 10. It is evident that in conditions without rain, due to incidental coherence effects over the receiver pupil (38 mm diameter), strong interferences are occurring. These events have a very short duration; consecutive samples may differ considerably. The consequence is that in the Fourier spectrum of the same data sets, as shown in Figure 15 (right), the spectral values for higher frequencies are dropping off rather slowly. The spectral band shown in the figure is ranging from 1 to 15 Hz. It is recommended to apply a higher sampling frequency in future experiments.

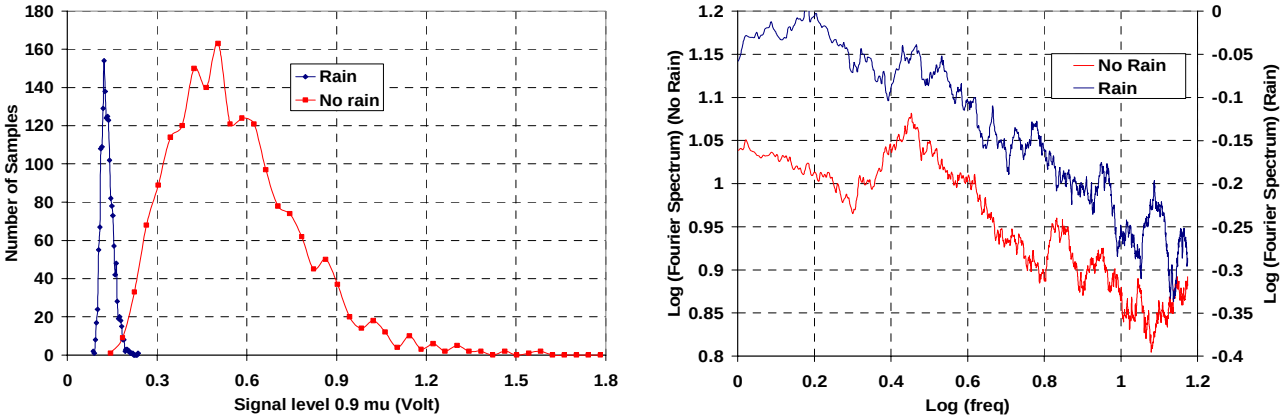


*Figure 15: Histograms (left) and Fourier transforms (right) of the τ data with/without rain for periods of about one minute.*

## 5.2 SCINTILLATION AND BEAM WANDER

For analysis of turbulence aspects, in the period from 3 June until 15 June recordings were made with an interval of 10 minutes for 2 seconds long with 25 Hz frames. Hence image sequences were recorded with 50 Hz fields, with a CCIR camera equipped with a 1250 mm Celestron telescope (12.5 cm lens diameter). This system has a 6.7 microradian spatial resolution. The equipment was installed at a height of 8.6 m at IMT and a light source of 8.6 cm diameter was located at a height of 7.5 m in Muizenberg (Whale watchers apartments) at a distance of 9.7 km. The sensor was located inside the building with an opened window to avoid platform motion due to strong winds.

Data reduction was performed for analysis of refraction, blur, beam wander as well as for scintillation. For the spatial position analysis (beam wander) the exact intensity levels are of less importance. Saturation and peak intensity signals as weight factors are therefore of less importance. Hence there are no criteria for using these items for data selection. The only criterion is that there are sufficient data for analysis, hence at least one data point per sequence. A lower number of accurate data point would result in processed data with less accuracy. A very limited amount of data was unusable when only a single position was determined with precision in the sequence.

For scintillation analysis there should be sufficient data points of sufficient quality. It turns out that saturation is not allowed to a high extend, and that data should be of sufficient quality to allow accurate averaging of the data. The criteria we have used allowed a maximum of 10 saturated images within a 100 samples and a maximum of 1 undetected (hence very low transmission) point in each 100 samples taken per image burst. These limits were established using practical analysis, when scintillation indices raised over-saturated values of about 0.4-0.5. Hence these data may be lowering the total scintillation effects measured.

In Figure 16 we present a comparison of the scintillation index ($\sigma^2/\langle I\rangle^2$, i.e. the ratio of variance and squared average intensity) from the Celestron and MSRT measurements. These set-ups were recording continuously during the trials. Data had to be selected carefully, as slight intensity errors can hamper the analysis. From the data we see that both data sets do indeed show a strong degree of correlation. Concerning the differences between the two data sets, we still need to consider the different paths, and different recording and analysis approaches.

Additional scintillation recordings were performed on the same source but from the IMT roof making use of a Marlin digital camera equipped with a 400 mm lens. This data are not shown here. Although there also correspondence between beam wander and scintillation index, this is not evident in the figure.

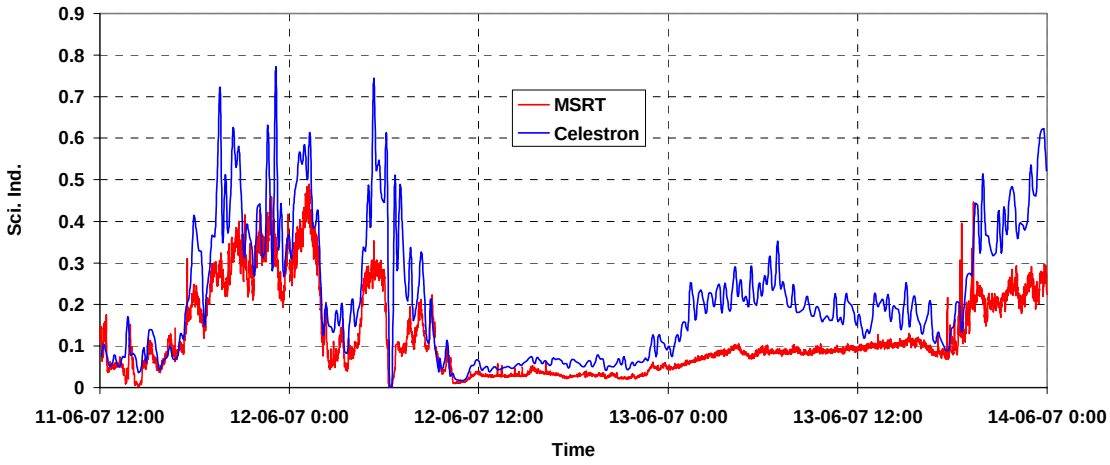


*Figure 16: Scintillation index of the Celestron spot images and MSRT point recordings over part the trial period.*

## 5.3 REFRACTION EFFECTS

We have obtained refraction recordings from a 15.7 km path from Rescue Station in Strandfontein to IMT, and from Muizenberg to IMT over 9.7 km. The first data was recorded with a Topcon imager (source at 8.7 m, imager at 7.9 m height) and the latter with a Celestron based CCD camera (the same equipment that was used for scintillation measurements and beam wander). In Figure 17 we present all the data. These paths also differ in azimuth direction. For the Topcon source configuration the expected horizontal cross-wire of the Topcon will be at a height of 27.3 m at the

location of the source. This equals to a difference between the horizontal and the source of 1.185 mrad. However due to neutral pressure and temperature profiles one might expect a tilt in the source path that changes the difference to 0.971 mrad.

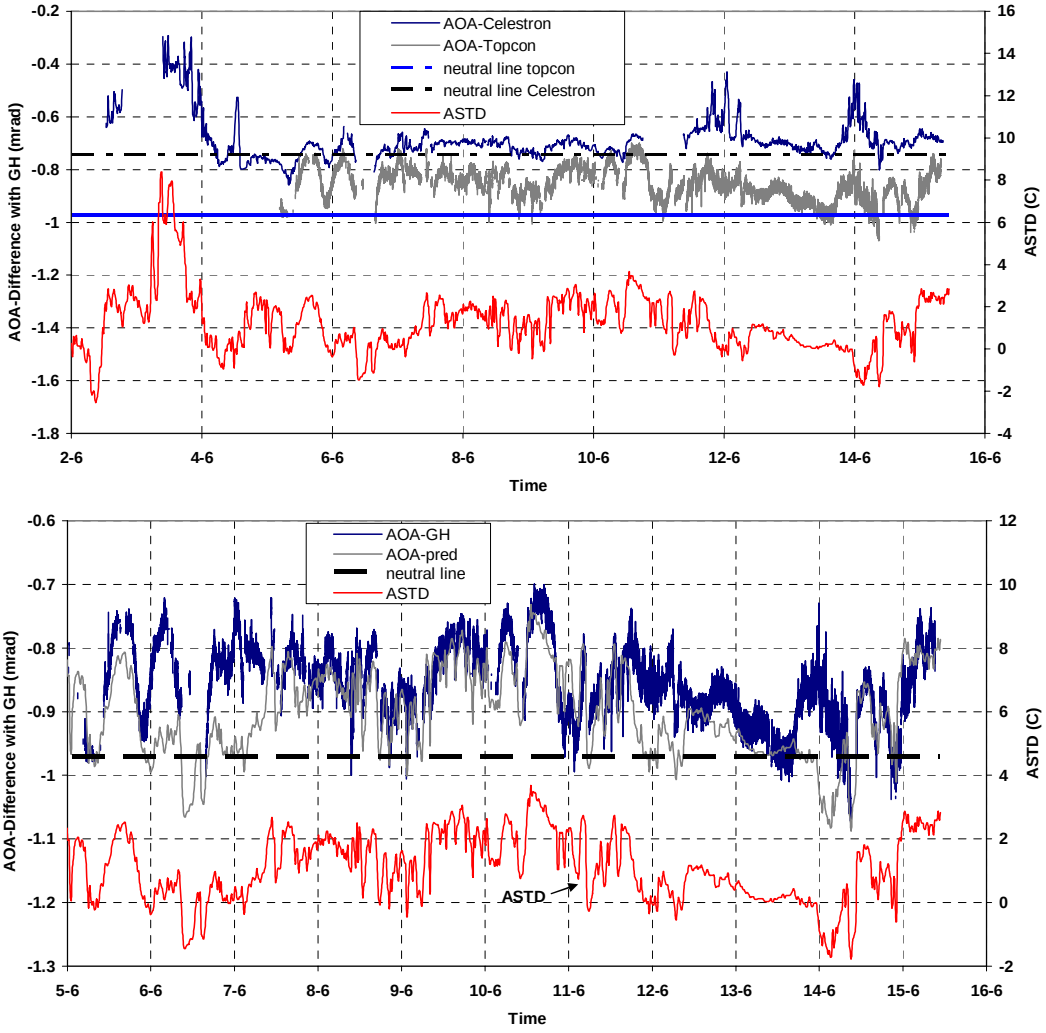


*Figure 17: Angle-of-Arrival measurements of the Topcon and Celestron imagers, compared with ASTD and model calculations for AOA.*

From Figure 17 we observe a correlation between ASTD (air-sea temperature difference) and the spot elevations for both imagers. The data from the two imagers also corresponds very well with each other in qualitative terms. This figure also show a good correlation on 3 June, where high ASTD values (due to a high air temperature) coincide with high spot elevations measured with the Celestron imager. Blank areas in the graphs indicate missing data for the different sensors. The upper graph of the figure also contains the neutral elevation positions for the two imagers, with the short path Celestron data to be expected somewhat higher than the longer path Topcon data. Almost all data are more or less exceeding the neutral position. The upper graph shows the data over the entire experimental period.
Based on the ASTD the expected angle of arrival was calculated for the Topcon data. These ray-tracing calculations were done for the path of 15.7 km between the Topcon camera at IMT and the sources at Strandfontein. The formula for the temperature profile was: $\Delta T = (ASTD)\ \{1-exp(-ah)\}$ with $h$ being the height and $a$ a scale-height parameter, for which a value of 0.8 was taken. This resulted in the approximation formula for the angle of arrival: $AOA = 65\ ASTD - 0.971$. The constant of 0.971 in this formula is the AOA value for neutral conditions, i.e. taking into account the hydrostatic pressure decrease with height and an adiabatic temperature decrease with height of 6°/km. This is compared

to the Topcon data in the lower graph in the figure. For a very large fraction of the data these two agree very well. Only at a few locations 6-8 June, 12 and 14 June the deviations are more severe (of the order of 0.1 mrad).

## 6. CONCLUSIONS

We have presented data that were derived during a common trial to investigate target contrast and contrast features of a number of small sea surface vessels. Data were recorded during different environmental conditions in False Bay in South Africa. A number of small vessels was recorded and analysed, including a rigid hull inflatable boat, a small scientific work boat, a small harbour patrol boat, a wooden whaler and swimmers. Recordings show a variation of contrasts due to solar illumination changes, temperature cooling by wind and by water spray, as well as sea surface variations due to sea state (white caps) and sun glint (solar reflections). Different backgrounds were recorded during the trial. Several examples of contrast calculations have been given. Some clearly show that the wake of the vessels can dominate the target contrast in different infrared and visual bands.
The trials took place under strongly varying circumstances. This has resulted in a wide variety of target data as well as a large dataset of interesting atmospheric conditions. The analysis of the atmospheric data shows that we have obtained accurate transmission data, a good correspondence between different approaches for scintillation measurements and promising refraction results. Refraction effects are well correlated with measured air-sea temperature differences, and our atmosphere model makes accurate predictions for the refraction. Decreased scintillation effects are present in case of lowered transmissions, and effects of rain on transmission are well captured in the recordings. Furthermore correlations between 0.6, 0.9 and 1.2 micron meter transmission data have been described.

## 7. ACKNOWLEDGEMENTS

The work for this paper was supported by the Netherlands MoD under the programme V602 “Electro-Optical sensor systems” and in South Africa by Armscor. The use of the National Sea Rescue Institute (NSRI) at Strandfontein, run by Wally Panday, as a location for sources and the Whale Watchers Beach Apartments (in the Empire building in Muizenberg), run by Mr. and Mrs. Robinson, as a location for sources and the MSRT is acknowledged. The South African Navy assisted with the execution of the trial and their support is gratefully acknowledged. Data analysis and number crunching at TNO was performed by Koen Benoist en Herman Bekman.

## 8. REFERENCES

1. Schwering, P.B.W., van den Broek, S.P., van Iersel, M., *EO System Concepts in the Littoral*, SPIE Proc. Vol. 6542 paper 100, 2007
2. Schwering, P.B.W., *IRST evaluation methodologies: Maritime infrared background simulator*, SPIE Proc. Vol. 6206, 620621, 2006
3. Schutte, K., de Lange, D.J.J., van den Broek, S.P., *Signal conditioning algorithms for enhanced tactical sensor imagery*, SPIE Proc. Vol. 5076, 92-100, 2003.
4. van den Broek, S.P., Bakker, E.J., de Lange, D.J., Theil, A; *Detection and classification of infrared decoys and small targets in a sea background*, 2000, SPIE Vol. 4029, 70-80, 2000
5. Theil, A., Huizing, A.G., van Heijningen, A.W.P., *Single Picture Integration for Territorial Waters Surveillance (SPITS): An initiative to improve situational awareness in littoral waters*, MAST (Maritime Systems and Technology) Conference, Nice France, 4-6 September 2006
6. Arie N. de Jong, Alexander M.J. van Eijk, Marcel M. Moerman, Leo H. Cohen, *Investigation of aerosol particle size distribution in the San Diego Bay by means of multi-band transmissometry*, SPIE Proc. Vol. 6303, August 2006
7. Arie N. de Jong, Alexander M.J. van Eijk, Peter J. Fritz, Leo H. Cohen, Marcel M. Moerman, *The use of multi-band transmission data, collected at Scripps pier in November 2007, for the investigation of aerosol characteristics*, SPIE Proc. Vol. 6708, August 2007